Asian Journal of Water, Environment and Pollution. Vol. 22, No. 6 (2025), pp. 73-88.
doi: 10.36922/AJWEP025120081

ORIGINAL RESEARCH ARTICLE

Machine learning-based discharge coefficient estimation in trapezoidal-arched labyrinth weirs

Mohammad Heidarnejad[1]*, Jamal Feili[2], Mehdi Fuladipanah[3], and Upaka Rathnayake[4]*

[1]Department of Water Science Engineering, Ahv. C., Islamic Azad University, Ahvaz, Iran
[2]Khuzestan Water and Power Organization, Ahvaz, Khuzestan, Iran
[3]Department of Civil Engineering, Ramh. C., Islamic Azad University, Ramhormoz, Iran
[4]Department of Civil Engineering and Construction, Faculty of Engineering and Design, Atlantic Technological University, Sligo, Connacht, Ireland

***Corresponding authors:** Mohammad Heidarnejad (mo.heidar@iau.ac.ir); Upaka Rathnayake (upaka.rathnayake@atu.ie)

Received: March 17, 2025; 1st revised: June 17, 2025; 2nd revised: July 8, 2025; Accepted: July 9, 2025; Published online: August 13, 2025

Abstract: Weirs represent a frequently employed mechanism for regulating water surface elevations and managing flow within canals and hydraulic infrastructures. Among these, labyrinth weirs constitute a distinctive variant capable of accommodating a specific discharge while maintaining a reduced upstream water level compared to conventional linear weirs. The present investigation delved into the evaluation of the effectiveness of multilayer perceptron (MLP) networks, support vector machine (SVM), gene expression programming (GEP), and multivariate adaptive regression splines (MARS), aiming to predict the discharge coefficient (C_d) of a trapezoidal-arched labyrinth weir with an expanded central cycle. A dataset including 108 laboratory observations was utilized. The dimensionless parameters were obtained from the parameters including inside apex width of the middle cycle (w_1), inside apex width of the end cycles (w_2), weir height on the upstream side (B), unsubmerged total upstream head on the weir (H_d), and gravitational acceleration (g). The model was developed with the dimensionless parameters and C_d. Root mean square error (RMSE), determination coefficient (R^2), mean absolute error (MAE), and developed discrepancy ratio (DDR) were used as performance assessment criteria. Based on these metrics, all four models exhibited the latent capacity to predict the C_d value. However, the MLP model demonstrated superior performance among the models during both training (RMSE = 0.024, MAE = 0.020, R^2 = 0.816, and $C_{d[DDRmax]}$ = 8.07) and testing (RMSE = 0.011, MAE = 0.006, R^2 = 0.688, and $C_{d[DDRmax]}$ = 11.32) phases. Sequentially, the subsequent standings were secured by the SVM, GEP, and MARS. MLP outperformed SVM, GEP, and MARS models in predicting C_d, achieving the highest R^2 and lowest RMSE/MAE values.

Keywords: Discharge coefficient; Laboratory observations; Machine learning models; Prediction; Trapezoidal-arched labyrinth weir

1. Introduction

Weirs, both linear and non-linear in configuration, are critical hydraulic structures designed for the regulation of excess flow and the precise management of water levels. These structures form an integral component of hydraulic systems, serving a pivotal role in flow regulation.[1] Engineering applications incorporate

weirs of various geometries, each exhibiting distinct hydraulic characteristics that significantly influence flow behavior.[2,3] Among these, labyrinth weirs represent a notable category widely employed in hydraulic engineering. These weirs are characterized by their intricate platforms, which often adopt geometric configurations such as triangular, rectangular, or trapezoidal shapes. The zigzag design of labyrinth weirs increases the effective crest length relative to linear weirs, thereby enhancing their discharge efficiency. This structural advantage enables them to convey larger volumes of water under lower upstream hydraulic heads. Furthermore, labyrinth weirs are recognized for their cost-effectiveness in terms of construction and operation.

The study of labyrinth weir hydraulics was initially undertaken by Gentilini,[4] who introduced triangular weirs by aligning several oblique weirs in sequence. Modern advancements in labyrinth weir design began with Taylor[5] and were subsequently refined by Hay and Taylor.[6] In 1985, the Bureau of Reclamation in the United States formalized a design methodology to assist engineers in designing and constructing labyrinth weirs for public infrastructure projects.[7] Meanwhile, Kocahan and Taylor[8] highlighted that labyrinth weirs, despite their passive flow control nature, can convey significantly higher discharge rates compared to standard ogee weirs during the initial stages of flood events. In a study, Crookston and Tullis[9] investigated the hydraulic efficiency of conventional and inverted labyrinth weirs in channels, concluding that orientation had no impact on performance. Subsequently, Christensen and Tullis[10] expanded the understanding of flow characteristics over arched labyrinth weirs, while Seamons[11] evaluated the effects of geometric variations on their efficiency and the accuracy of design predictions.

Due to the intricate three-dimensional flow patterns over labyrinth weirs, determining an exact analytical solution for the head-discharge relationship remains challenging. For example, Bijankhan and Kouchakzadeh[12] conducted experimental and theoretical studies on water flow through triangular plan labyrinth weirs under both free and submerged flow conditions. New experimental data were collected for free flow, while the transition threshold between free and submerged regimes was identified experimentally. Using Buckingham π analysis, a head-discharge relationship was developed for submerged flow. A step-by-step calibration method was introduced to derive a unified discharge coefficient (C_d) that applies across free flow, submerged flow, and the transition zone, allowing continuous application of the coefficient under varying flow conditions.

Monjezi *et al*.[13] emphasized the critical role of weirs in dam safety and investigated the C_d of direct and arched weirs in linear and triangular labyrinth forms through laboratory experiments. Arched weirs, due to their curved geometry, increase the effective crest length at a given width, enhancing discharge capacity. Results showed that increasing the ratio of total hydraulic load to weir crest height decreases C_d in all weirs. However, arched shapes improved efficiency by up to 21% in linear weirs and 57% in labyrinth weirs. However, higher hydraulic loads reduced arched weir efficiency due to increased downstream standing wave height.

Furthermore, Seyedian *et al*.[14] investigated the use of machine learning models (MLMs) to predict the C_d of triangular labyrinth weirs, a key parameter in flow control. They developed and evaluated three MLMs: least-square support vector machine (SVM), quantile regression forest, and Gaussian process regression (GPR). Using statistical and visual methods, they found that GPR outperformed the others, achieving a determination coefficient (R^2) of 0.986 and root mean square error (RMSE) of 0.009. Sensitivity analysis revealed the Froude number and weir geometry as the most influential inputs. Notably, GPR not only provided the highest accuracy but also offered reliable prediction intervals, making it the preferred model for C_d prediction.

In the study by Zare *et al*.,[15] they conducted an experimental study on inclined circular labyrinth weirs with inclination angles of 60°, 70°, 80°, and 90° and diameters of 15, 20, 25, and 30 cm under varying flow rates. The flow transitioned from free to submerged as discharge increased, with no air entrainment observed. Results showed that increasing the dimensionless ratio of total hydraulic head to weir height reduced the C_d. The 60° inclined weir achieved the highest C_d, while the vertical (90°) weir had the lowest. Although the 15 cm diameter weir initially exhibited the highest C_d, diameter changes had a minimal overall impact.

Similarly, Nematollahi *et al*.[16] analyzed eight sinusoidal labyrinth weirs with varying heights and effective crest lengths to study C_d and energy loss. Increasing flow rate or upstream depth decreased both metrics, while greater effective length and inlet-to-outlet width ratios increased them. Maximum energy loss occurred at width ratios of 4.60 and 7.67. A 20% increase in weir height led to a 19.8% increase in energy loss. Flow splitters reduced the C_d but increased energy loss. The study also provided equations for C_d and energy loss with high correlation coefficients.

Ahmed and Altalib[17] investigated the effects of cycle number, total arc angle, and semicircular openings on the C_d of arched weirs and arched labyrinth weirs. Reducing the number of cycles increased the C_d by up to 35.94%, with arched weirs performing better than arched labyrinth weirs. Increasing the total arc angle improved the coefficient by up to 32.4%. However, semicircular openings reduced performance, with C_d decreases of 19.54% for arched labyrinth weirs and 12.08% for linear weirs as the opening-to-edge length ratio increased. A predictive equation was developed to predict C_d, showing a strong correlation with experimental data (R = 0.9).

Masoudi *et al*.[18] emphasized the importance of flood discharge from dam reservoirs, typically managed using weirs. Labyrinth weirs, ideal for narrow valleys and large floods, offer high efficiency due to their extended flow paths. This study aimed to enhance the C_d and efficiency of rectangular and trapezoidal labyrinth weirs by replacing uniform, regular labyrinth cycles (congresses) with unequal and irregular ones. Five samples of each weir type were tested in two configurations, differing by the placement of the longest cycle (center vs. sides). Experimental results showed that using unequal and irregular congresses improved the C_d by 40.7% for rectangular weirs and 35.3% for trapezoidal ones.

Similarly, Hadi and Majeed[19] investigated the C_d of side weirs installed in the side wall of a rectangular channel, focusing on trapezoidal labyrinth weirs with side wall angles of 15°, 30°, 45°, 60°, 75°, and a linear side weir at 90°. Using six physical models, they developed hydraulic equations relating discharge and head over the weir. Results showed that the C_d increases with larger side wall angles and is highest at 75°, approaching the value for a straight (90°) weir. Computational fluid dynamic simulations using the k-omega shear stress transport model and volume of fluid scheme confirmed the experimental findings, showing strong agreement.

Non-linear weirs demonstrate a superior overflow capacity relative to linear weirs, attributable to their extended crest length. The C_d plays a critical and notable role in the hydraulic performance of non-linear weirs. The usual discharge equation for a labyrinth weir is given in Equation I.

$$Q=\frac{2}{3}C_d L_c \sqrt{2g} H_T^{1.5} \quad (I)$$

where Q is the overflow rate, Lc is the effective crest length, H_T denotes the total upstream head, and g is the acceleration due to gravity. The C_d values are influenced by hybrid hydraulic-geometry parameters, prompting numerous studies and research endeavors to elucidate this effect. Table 1 summarizes a list of C_d predictors presented by various researchers.

The adoption of recently developed MLMs as a state-of-the-art approach has supplanted the need for costly, limited, and time-intensive experimental tests. MLMs employ training and testing phases to uncover intricate and hidden relationships between dependent and independent variables, thereby facilitating accurate forecasting of target variables.[27] Table 2 presents a comprehensive summary of various studies aiming to predict the C_d in overflows of differing shapes.

As evident from Table 2, accurately determining the C_d for structures such as labyrinth, piano-key, and lateral weirs has long been a focus of research due to its potential to enhance performance efficiency. The use of MLMs has demonstrated superior accuracy compared to traditional regression models and empirical equations. In addition, the exploration and development of new configurations inspired by the geometry of the labyrinth weir is a burgeoning area of study. To address these aspects, this study employs four MLMs–SVM, gene expression programming (GEP), artificial neural network (ANN), and multivariate adaptive regression splines (MARS)–to simulate the C_d of a trapezoidal-arched labyrinth weir (TALW). A review of existing literature reveals a gap in research specifically focused on this topic.

2. Materials and methods

2.1. Data series

The experimental procedures for this research were conducted in the hydraulic laboratory of the Khuzestan Water and Power Authority, Iran. The weir models were installed within an 8 m long, 0.6 m wide, and 0.6 m high test flume with transparent Plexiglas walls, facilitating the observation of water surface profiles and flow conditions. The flume was operated under free-flow conditions. To ensure the accuracy of the results, the flume was designed to be watertight and seamless. The test equipment and components of the flume comprised the flume's groundwater tank, a digital flowmeter with an accuracy of 0.2 L/s, a tranquilizer, a floating electric pump with a maximum flow rate of 140 m^3/h, and a constant-head tank (Figure 1A). The digital magnetic flowmeter was calibrated against a 90° V-notch weir installed at the flume outlet. The weir's

Table 1. Summary of predictive equations for the discharge coefficient of labyrinth weirs

References	Equation	Recommendation
Darvas[20]	$C_d = \frac{Q_{max}}{Wh_{max}^2}$ (II)	Triangular labyrinth weir; $0.2 \le \frac{H_T}{P} \le 0.6$; side wide angle $\ge 0.8\alpha_{max}$
Lux and Hinchliff[21]	$C_d = \frac{Q_{cycle}}{\frac{\frac{w}{P}}{\frac{w}{P}+k} w\sqrt{g}H_T^{1.5}}$ (III)	Labyrinth weir with one cycle; $\frac{w}{P} > 2$; k is the apex shape constant
Melo *et al.*[22]	$C_d = \frac{Q}{k_{,-CW} W\sqrt{2g}H_T^{1.5}}$ (IV)	Circular labyrinth weir; $1 \le k_{\theta\text{-}CW} \le 1.4$
Crookston[23]	$C_d = A(\frac{H_T}{P})^{(B(\frac{H_T}{P})^C)} + D$ (V)	Labyrinth weir with half-round and quarter-round crests; A, B, C, and D are curve-fit coefficients; $6 \le \alpha \le 35$
Emiroglu *et al.*[24]	$C_d = (18.6 - 23.535[\frac{L}{B}]^{0.012} + 6.769[\frac{L}{l}]^{0.112} - 0.502(\frac{W}{y_1})^{4.024} + 0.094\sin_{,} - 0.393Fr_l^{2.155})^{-1.431}$ (VI)	Triangular labyrinth weir with one cycle
Karami *et al.*[25]	$C_d = 0.012(\frac{y_1}{W})^{-2.5} + 0.881r_{,}^{0.248} + 2.97Fr_2^{1.79}$ (VII)	Asymmetric triangular with one cycle
Bonakdari *et al.*[26]	$C_d = 0.466 + 0.388\frac{P}{y} - 0.183\frac{L}{W} - 0.022\frac{L}{y} + 0.31Fr + 0.12\sin\theta$ (VIII)	Triangular labyrinth weir

discharge equation ($Q = 1.417 \cdot H^{2.5}$) was validated, with head measurements accurate to ±0.1 mm. Calibration tests across the experimental flow range (5–50 L/s) confirmed flowmeter deviations within ±0.15 L/s, ensuring high-fidelity discharge data. The bottom of the flume was a fixed-bed type and maintained as horizontally as practically possible.

Water was initially pumped from the groundwater tank into the head tank, from where it flowed through a 0.3 m diameter pipe toward the inlet of the test flume, regulated by a globe valve. Water entered the flume at a low flow rate, gently passing over the weir. By varying the flow rate, the hydraulic conditions at the upstream, over, and downstream of the weir were recorded. Ultimately, water exited the flume into a downstream channel, entered the pumping tank, and was recirculated back into the system. A representation of the geometry dimension is illustrated in Figure 1B. A series of 120 tests was conducted using 12 models of TALW with an expanded middle cycle. Table 3 represents parameters included for the tests.

A schematic representation of the labyrinth weir is provided in Figure 2, detailing its geometric parameters relative to the weir crest. A represents the inside apex width, t_w indicates the wall thickness, α is the sidewall angle, W corresponds to the apron width, w denotes the cycle width, P represents the weir height, and T indicates the pier thickness.

2.2. Dimensional analysis

The values of C_d for TALW can be considered a function dependent on the following parameters:

$$C_d = F(Q, w_1, w_2, B, H_d, g) \quad \text{(IX)}$$

Where Q is the flow rate, w_1 is the inside apex width of the middle cycle, w_2 is the inside apex width of the

Table 2. Summary of machine learning model applications to predict discharge coefficient

References	MLMs included	Weir type	Findings
Mahmoud *et al.*[28]	HI-MLP, ANFIS, SVR, MLP, GA	LW	HI-MLP demonstrates the highest accuracy.
Nourani *et al.*[3]	SVM-PSO, GA, SVM-GA	CCOW	The SVM-GA hybrid model outperforms the others.
Emami *et al.*[29]	Hybrid (LSHADE- XGB), ANFIS, GEP, SAELM, ANN	PCLW	The hybrid model demonstrates higher accuracy.
Majedi-Asl *et al.*[30]	SVM, GEP	PKW, LW	GEP demonstrates higher accuracy.
Mustafa *et al.*[31]	NLR, BPNN, GA, PSO	TSLW	GA-BPNN and PSO-BPNN exhibit notably accurate prediction results.
Wang *et al.*[32]	ANFIS, SVM, M5-tree, LSSVM, LSSVM-BA	CLW	LSSVM-BA demonstrates the highest accuracy during the training and testing phases.
Hu *et al.*[33]	CFD; ANFIS, ANFIS-FA	LW	ANFIS-FA demonstrates significantly higher accuracy.
Mahmoud *et al.*[34]	SAELM	NLW, ILW	SAELM exhibits reasonable accuracy.
Shafiei *et al.*[35]	LSSVM, ELM, BELM, LR	PKW	BELM demonstrates excellent performance.
Norouzi *et al.*[36]	SVM	LW, ALW	The SVM-based model demonstrates higher accuracy.
Olyaie *et al.*[37]	ANN, GP, ELM	TLW	ELM demonstrates superior performance.
Roushangar *et al.*[38]	LGP, MLR, NLR	RSW	Mathematical models demonstrate higher accuracy.
Uyumaz *et al.*[39]	ANFIS, ANN, NLR, MLR	TLSW	ANFIS is more successful in modeling.
Emiroglu and Kisi[40]	ANFIS, NLR	SESW	ANFIS demonstrates higher accuracy.

Abbreviations: ALW: Arched-labyrinth weir; ANFIS: Adaptive neural-fuzzy inference system; ANN: Artificial neural network; BA: Bat algorithm; BELM: Bayesian extreme learning machine; BPNN: Back-propagation neural network; CCOW: Circular-crested oblique weir; CFD: Computational fluid dynamics; CLW: Curved labyrinth weir; ELM: Extreme learning machine; FA: Firefly algorithm; GA: Genetic algorithm; GEP: Gene expression programming; GP: Genetic programming; HI-MLP: Hydraulic-informed multilayer perceptron; ILW: Inverted orientation labyrinth weir; LGP: Linear genetic programming; LM: Levenberg–Marquardt algorithm; LR: Logistic regression; LSHADE: Linear population size reduction history-based adaptive differential evolution; LSSVM: Least-square support vector machine; LW: Labyrinth weir; MLP: Multilayer perceptron; MLR: Multiple linear regression; NLR: Non-linear regression; NLW: Normal orientation labyrinth weir; PCLW: Pseudo-cosine labyrinth weir; PKW: Piano key weir; PSO: Particle swarm optimization; RBFNN: Radial basis function neural network; RSW: Rectangular side weir; SAELM: Self-adaptive extreme learning machine; SESW: Semi-elliptical side weir; SVR: Support vector regression; TLSW: Trapezoidal labyrinth side weir; TSLW: Triangle shape of labyrinth weir; XGB: Extreme gradient boosting algorithm.

end cycle, B is the weir height on the upstream side, H_d is the unsubmerged total upstream head on the weir, and g is the gravitational acceleration. These parameters collectively inform the calculation of C_d and capture the complex interactions between hydraulic and geometric factors that affect the flow behavior of these structures. For conducting dimensional analysis, the parameters P, g, and Q were identified as repeating variables, leading to the derivation of dimensionless parameters as outlined in Equation X.

$$C_d = F\left(\frac{H_d}{B}, \frac{gB^5}{Q^2}, \frac{w_1}{B}, \frac{w_2}{B}\right) \quad (X)$$

The influence of the gravitational acceleration $\frac{gB^5}{Q^2}$, which represents the Froude number, is incorporated through the dimensionless parameter $\frac{H_d}{B}$. Given these conditions, Equation X is simplified to the following Equation XI:

$$C_d = F\left(\frac{w_1}{B}, \frac{H_d}{B}, \frac{w_1}{w_2}\right) \quad \text{(XI)}$$

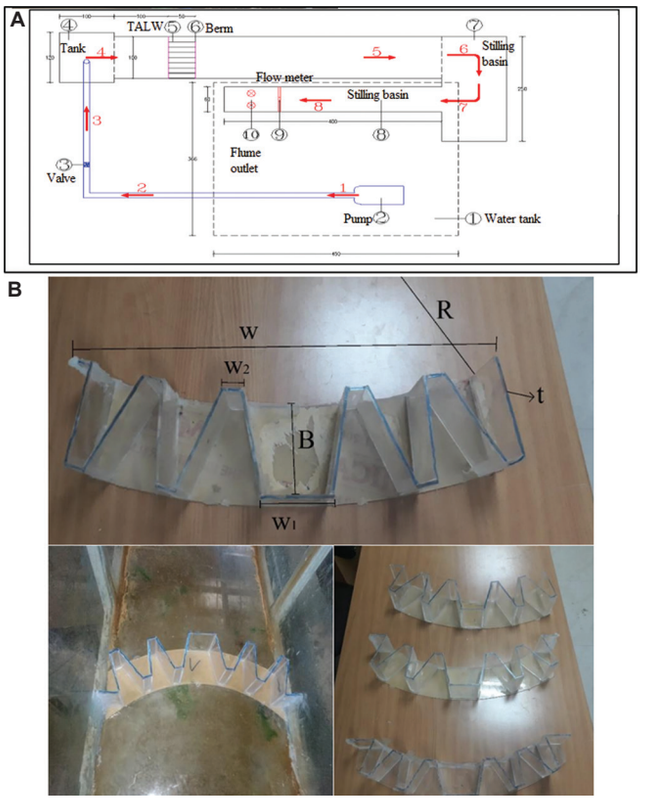

Figure 1. Flume and weirs model of experiments: (A) Plan view of the setting. (B) Geometry parameters of the trapezoidal-arched labyrinth weirs (TALWs)
Notes: B is the weir height on the upstream side; R is the arc radius; t is the crest thickness; W is the width of a cycle; W_1 is the inside apex width of the middle cycle; W_2 is the inside apex width of the end cycle.

2.3. MLMs

2.3.1. SVM

Developed by Cortes and Vapnik,[41] the SVMs are a class of supervised learning methods used for classification and regression tasks in machine learning. They are particularly well-suited for binary classification problems, though extensions to multiclass classifications exist. The core concept behind SVM is the construction of hyperplanes in a high-dimensional space that can be used to separate different classes of data points.[38] Given a training dataset $\{(X_i, y_i)\}_{i=1}^{N}$, where $X_i \in \mathbb{R}^n$ represents the feature vectors and $y_i \in \{-1,1\}$ represents the class labels, the objective of SVM is to find a hyperplane that maximally separates the two classes.[42]

To model a problem using SVM, the first step is to clearly define the problem by determining whether it is a classification, regression, or outlier detection task. Once the task is identified, the next step involves collecting and preprocessing the dataset to ensure that the data are clean, normalized, and suitable for modeling. Based on the nature and structure of the data, an appropriate kernel function is then selected to transform the input space if necessary. After selecting the kernel, the dataset is split into training and testing sets, typically using an 80:20 ratio, to evaluate the model's performance on unseen data. The next step is to set the key hyperparameters of the SVM model. These include the regularization parameter C, which controls the trade-off between achieving a wide margin and minimizing classification errors, and other kernel-specific parameters, such as γ for the radial basis function (RBF) kernel or the degree for polynomial kernels. With the data prepared and parameters set, the model is trained using the training dataset. During training, the SVM algorithm attempts to maximize the margin between classes in classification

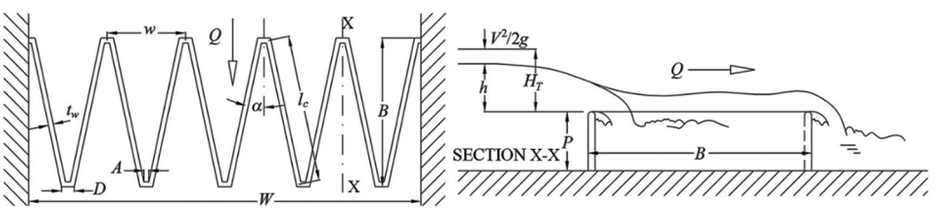

Figure 2. Shape and geometric parameters of the labyrinth weir
Notes: α is the wall angle; A is inside apex width, X-X is cross section of the weir; B is the weir length; D is the apex width; H is the depth head; H_t is the total upstream head; h_t is the velocity head; L_c is the wall length; P is the weir height; Q is the flow discharge; T is the weir height; t is the crest thickness; W is the total width; w is the width of a cycle.

Table 3. Summary of hydraulic and geometric parameters

No.	W (cm)	R (cm)	L (cm)	t (mm)	N	$\frac{w_2}{w_1}$	$\frac{B}{w_1}$	Q (L/s)
1	60	45	66	5	-	-	-	5–50
2			136		5	0.42	1.00	
3			136			0.35	1.00	
4			136			0.30	1.00	
5			152			0.42	1.25	
6			152			0.35	1.25	
7			152			0.30	1.25	
8			170			0.42	1.50	
9			170			0.35	1.50	
10			170			0.30	1.50	

Notes: B is the weir height; L is the weir length; N is the number of cycles; R is the arc radius; t is the crest thickness; W is the width of a cycle; W_1 is the inside apex width of the middle cycle; W_2 is the inside apex width of the end cycle.

tasks or fit a hyperplane within an ε-insensitive region in regression tasks. Following training, model validation is conducted through cross-validation to assess performance and identify opportunities for improvement. Hyperparameters are then fine-tuned using techniques such as grid search or random search. Finally, the model is evaluated on the testing dataset using appropriate evaluation metrics, including accuracy, precision, recall, F1-score for classification tasks, and RMSE and mean absolute error (MAE) for regression tasks. This final evaluation provides insights into the model's generalization capability and overall effectiveness.

2.3.2. GEP

The GEP is an evolutionary algorithm that creates models and solutions by evolving computer programs or expressions. Developed by Ferreira,[43] the GEP is an extension of genetic programming and genetic algorithms. It combines the strengths of both approaches to effectively solve complex problems in various fields, including artificial intelligence, bioinformatics, and engineering.

Chromosomes and expression trees (ETs), functions and terminals, and fitness functions are three fundamental concepts of the GEP. Chromosomes in GEP are linear strings of fixed length composed of genes, which encode the solutions. Each gene consists of a head and a tail. The head contains functions and terminals, while the tail contains only terminals. These linear chromosomes are translated into ETs, which are the functional representation of the chromosome. ETs are hierarchical structures that represent the solution in a form that can be evaluated. On the other hand, functions are mathematical operations (e.g., addition and subtraction) or logical operations, while terminals are variables or constants that serve as the input for the functions. A fitness function evaluates how well a chromosome solves the problem at hand. It compares the output of the ET with the desired output, assigning a fitness score to each chromosome.[44]

To begin modeling with GEP, the first step is to clearly define the problem, whether it involves regression, classification, or symbolic modeling. After identifying the problem type, a suitable dataset is collected and carefully preprocessed to handle missing values and normalize or standardize features if necessary, ensuring the data quality supports accurate modeling. Once the data is ready, the next step is to split it into training and testing subsets – typically allocating 70–80% of the data for training and the remainder for testing, which allows for evaluation of the model's predictive capability. With the data split, the structure of the GEP model is configured by setting parameters such as the number of genes, head size, function set (e.g., mathematical operators like +, –, *, and/), and terminal set (input variables and constants). The evolutionary process then begins, during which a population of random solutions is generated and evolved over several generations using genetic operators, such as mutation, transposition, and recombination. The fitness of each chromosome is evaluated based on fitness functions, such as mean squared error for regression and classification accuracy for classification tasks. Through successive generations, the population evolves to produce increasingly accurate solutions. Once the model training is complete, the optimally evolved expression or model is selected, and its performance is evaluated on the testing dataset using appropriate metrics. Finally, the resulting symbolic expression can be interpreted and, if necessary, simplified for use in practical applications or further analysis.[45]

2.3.3. ANN

The ANN stands as an advanced mathematical approach proficient in mapping intricate systems rooted in datasets. A prevalent category of ANN is the multilayer perceptron (MLP), which is extensively employed in research studies. The effective deployment of an MLP model necessitates the specification of suitable transfer functions and the configuration of an optimal structure,

taking into account computational efficiency. It is plausible to assess diverse transfer functions to identify the most appropriate one. An ANN may encompass one or more hidden layers. After finalizing the MLP structure (including the number of hidden layers and the number of neurons within each hidden layer), the determination of weights and biases ensues, a phase referred to as model training.[46]

The process of the MLP model design entails a sequence of strategic stages:

(i) Evaluation of hidden layer count: The initial phase involves assessing the optimal number of hidden layers in the network architecture
(ii) Determination of neuron quantity in each layer: The second step entails deciding on the suitable number of neurons within each hidden layer
(iii) Specification of transfer functions: The identification of appropriate transfer functions for neuron activations is pursued
(iv) Selection of training algorithm: The selection of an effective training algorithm for network optimization concludes the design process.

To achieve an optimal MLP model configuration, a systematic approach is adopted. Initially, a single hidden layer is proposed, where the neuronal count aligns with the quantity of input features. Subsequently, various transfer functions, such as log-sig, tan-sig, and pure-line, are systematically assessed. Once an appropriate activation function is determined, the augmentation of predictive precision is pursued. This entails the progressive elevation of the count of hidden layers and neurons within these layers, thereby capturing intricacies within the data and refining model performance through an iterative refinement process.[47]

2.3.4. MARSs

The inception of MARS, attributed to Friedman,[48] has permeated various branches of engineering, particularly hydraulic engineering, demonstrating broad utilization. MARS is an adaptable tool, facilitating the establishment of relationships between independent and dependent variables within a targeted system. By leveraging the MARS method, latent patterns within complex datasets are discerned, unveiling hidden insights in intricate designs. The pattern recognition process involves the proposal of a range of coefficients and basis functions, validated through regression operations performed on the relevant dataset. A key strength of the MARS lies in its aptitude for effectively mapping input parameters to desired outputs, constructing uncomplicated yet resilient models, and offering a judicious balance in computational expense.[49]

To simulate and model a problem using the MARS algorithm, the first step is to define the objective of the modeling process, whether it involves predicting a continuous variable (regression) or classifying data. Once the problem is clearly understood, a relevant dataset is collected and preprocessed by handling missing values, removing outliers if necessary, and normalizing or scaling the features to ensure consistent input data. After preparing the dataset, it is typically divided into training and testing sets to allow for subsequent performance evaluation. The MARS model is then initialized by selecting key parameters, such as the maximum number of basis functions, the degree of interactions allowed between variables, and any penalties for model complexity to prevent overfitting.

The training process begins by allowing the model to construct a set of piecewise linear basis functions, which adaptively split the data at optimal points (called knots). MARS adds these functions in a forward stepwise manner to minimize residual error and capture non-linear relationships and interactions between variables. After building a complex model in the forward phase, a backward pruning process is applied to eliminate redundant or less important basis functions, resulting in a simpler and more generalizable model. Once training is complete, the model's performance is evaluated using the testing dataset. Finally, the resulting MARS model yields an interpretable set of rules or functions that describe the underlying patterns in the data, rendering it useful for both predictions and understanding variable relationships.[50]

2.4. Performance assessment criteria of MLMs

Several key metrics were used to assess the effectiveness of the employed algorithms in ML prediction and forecasting models. These metrics encompassed the R^2, the RMSE, the MAE, and the developed discrepancy ratio (DDR), as detailed in Equations XII-XV.[51]

$$R^2 = \frac{\sum_{i=1}^{N}(O_i - \bar{O})(P_i - \bar{P})}{\sqrt{\sum_{i=1}^{N}(O_i - \bar{O})^2}\sqrt{\sqrt{\sum_{i=1}^{N}(P_i - \bar{P})^2}}} \quad \text{(XII)}$$

$$RMSE = \sqrt{\frac{\sum_{i=1}^{N}(O_i - P_i)^2}{N}} \quad \text{(XIII)}$$

$$MAE = \frac{\left|\sum_{i=1}^{N}(O_i - P_i)\right|}{N} \quad \text{(XIV)}$$

$$DDR=\frac{P}{O}-1 \quad \text{(XV)}$$

Where O and P are observed and predicted values, respectively; $\bar{O}$ and $\bar{P}$ are the mean of the observed and the predicted values, respectively; and N is the total dataset number. The first three criteria assess the mean error values associated with the implemented models. To address this deficiency, Noori *et al*.[51] introduced the DDR index. To enhance interpretation and visualization, the Gaussian distribution of DDR values should be depicted as a standard normal distribution. To achieve this, two steps are followed. First, the DDR values (C_d) are standardized, resulting in the calculation of the normalized DDR value ($C_{d[DDR]}$) using a Gaussian function. Second, a plot is created, where $C_{d(DDR)}$ values are plotted against their standardized counterparts (Z_{DDR}). In the Z_{DDR} vs. $C_{d(DDR)}$ graph, a greater alignment of error distribution toward the centerline and larger $C_{d(DDR)}$ values indicate increased accuracy.

2.5. Overall methodology

Machine learning prediction models were developed using the discussed SVM, GEP, ANN, and MARS methods. Of the aggregate data gathered from the experiments, the proportions allocated for the phases of the model's training and testing were 70% and 30%, respectively. The developed models were then tested for their performance as per the metrics given in Equations XII-XV.

3. Results and discussion

Table 4 presents an overview of the statistical performance criteria for the predicted models. For the establishment of the SVM, an evaluation was conducted on both the RBF and the polynomial kernel function. Subsequent testing of these kernel functions revealed that the RBF kernel function outperformed the polynomial function. In the SVM setup, the values of tuning parameters C and γ were determined as 67 and 5.5, respectively. The values of RMSE, MAE, R^2, and $C_{d(DDRmax)}$ during both the training and testing phases were as follows: 0.02679, 0.02318, 0.79808, and 7.50, respectively; and 0.0113, 0.0066, 0.7573, and 10.36, respectively.

Table 5 summarizes the setting parameters of the superior GEP model. The values for RMSE, MAE, R^2, and $C_{d(DDRmax)}$ were observed as follows: 0.03847, 0.03275, 0.74962, and 5.35, respectively, during the training phase and 0.0181, 0.0109, 0.5624, and 6.32, respectively, during the testing phase. The operators involved in the GEP are +, −, ×,/, √, e^x, ln, x^2, x^3, $x^{\frac{1}{3}}$. Figure 3 demonstrates the ET of the GEP output. The corresponding values in Figure 3 are G1C1 = −0.476807, G2C0=2.40567, G2C1=−0.476807, G3C0=−0.395355, G3C1 = −0.665436. It is worth noting that d0, d1, and d2 stand for $\frac{B}{w_1}$, $\frac{H_d}{P}$, and $\frac{w_1}{w_2}$, respectively.

The MLP model in this study has the following performance metric values (RMSE, MAE, R^2, and $C_{d[DDRmax]}$) associated with it: 0.02426, 0.02031, 0.81602, and 8.07, respectively, during the training phase, and 0.0111, 0.0065, 0.6878, and 11.32, respectively, during the testing phase. The last model employed in this investigation is the MARS model, with performance metrics reaching 0.04995, 0.04381, 0.51011, and 4.02, respectively, during the training phase and 0.0245, 0.0149, 0.5593, and 4.64, respectively, during the testing phase. In the process of the MARS model development, an initial set of 21 basis functions was taken into account during the first step. Subsequently, during the second step (pruning step), 18 of these basis functions were removed. Ultimately, the optimal MARS model, consisting of three basis functions, was obtained. The representation of the acquired MARS model is presented in Equation XVI, while the elaborated representation is detailed in Table 6.

Table 4. Summary of the model performance

Model	Training phase				Testing phases			
	RMSE	MAE	R^2	$C_{d\ (DDRmax)}$	RMSE	MAE	R^2	$C_{d\ (DDRmax)}$
SVM	0.02679	0.02318	0.79808	7.50	0.0113	0.0066	0.7573	10.36
GEP	0.03847	0.03275	0.74962	5.35	0.0181	0.0109	0.5624	6.32
MLP	0.02426	0.02031	0.81602	8.07	0.0111	0.0065	0.6878	11.32
MARS	0.04995	0.04381	0.51011	4.02	0.0245	0.0149	0.5593	4.64

Notes: R^2 is the determination coefficient; $C_{d\ (DDRmax)}$ is the maximum normalized developed discrepancy ratio value.
Abbreviations: GEP: Gene expression programming; MAE: Mean absolute error; MARS: Multivariate adaptive regression splines; MLP: Multilayer perceptron; RMSE: Root mean square error; SVM: Support vector machine.

Table 5. Tuning parameters of the gene expression programming model

Parameter	Value/description
Population size	110
Number of genes	3
Gene head length	10
Gene tail length	11
Mutation rate	0.044
Inversion rate	0.1
Gene transposition rate	0.1
One point recombination rate	0.3
Two-point recombination rate	0.3
Gene recombination rate	0.1
Fitness function	Root mean square error

Table 6. Multivariate adaptive regression splines model's basis functions and their corresponding coefficients

Basis function	Coefficient	Equation
$h_1(x)$	0.0025329	$\text{Max}\left(0, 0.00765854 - \frac{H_d}{P}\right)$
$h_2(x)$	−0.0012013	$\text{Max}\left(0, \frac{B}{w_1} - 1\right)$
$h_3(x)$	0.0020736	$\text{Max}\left(0, \frac{w_2}{w_1} - 0.003\right)$

$$C_d = 0.00409658 + \sum_{i=1}^{3} {}^{2}{}_{m} h_m(X) \quad \text{(XVI)}$$

Figure 4 presents a comparative analysis of the performance of the four distinct models, evaluated through the distribution of data points along a line with a 1:1 slope, during both the training and testing phases. Enhanced model performance is indicated by reduced proximity to this reference line. In the testing phase, the output data of the GEP and MARS models exhibit a notable deviation from the ideal line. In contrast, the MLP and the SVM models demonstrate data distribution closer to the reference line, suggesting their superior performance. The MLP model demonstrates a relatively higher efficacy than the SVM model due to its data's closer alignment with the 1:1 reference line. In general, it can be inferred that among the four models under consideration, the MLP model exhibits greater consistency with the actual measured C_d values. In the data distribution plot of the testing phase, the outcomes unequivocally demonstrate the supremacy of the MLP model in comparison to the remaining three models.

Table 7 presents the statistical indices of the residual values for the output of each of the four MLMs employed in this study during both the training and testing phases. As observed, the MLP model exhibits the lowest deviation in both phases, indicating superior performance in terms of consistency and accuracy. On the other hand, the MARS model shows the highest error in estimating C_d among the four models. The mean prediction errors for the MLP model during the training and testing phases are −0.002 and 0.002, respectively – these are the lowest values among all evaluated models. Conversely, the MARS model demonstrates the highest deviation in this metric. The total residual error for the MLP model is −0.14 in the training phase and 0.086 in the testing phase, which are also the smallest among the models, further confirming its accuracy and robustness. Overall, analysis of the residual error values clearly indicates that the MLP model provides higher prediction accuracy for C_d compared to the other models.

A graphical representation of the residual error variations during the training and testing phases for all four MLMs is provided in Figure 5. In this figure, the residual error values for the MLP model are highlighted in red. As can be seen, the MLP model's errors are closest to the horizontal axis, indicating the highest accuracy (i.e., the smallest deviation) among all models.

Figure 6 presents a comparative evaluation of model performance in the training and testing phases, assessed using the DDR index. As elucidated in the index description, elevated values along the vertical axis, coupled with a bell-shaped curve in its vicinity, signify enhanced performance. Based on these criteria, the MLP model exhibits the best performance in the training and testing phases. The values of $C_{d(DDRmax)}$ for the training and testing stages are 8.07 and 11.32, respectively. Subsequently, the SVM, GEP, and MARS models sequentially secure the second to fourth positions in terms of performance ranking.

Predicting C_d of different weirs is important due to various hydraulic and environmental reasons. The C_d governs the flow over the weirs; therefore, it determines the efficiency of flow, which can be handled over the weir. The flood water discharges or diversion over the weir can be efficiently and optimally controlled through accurate prediction of the weir C_d. Labyrinth weirs are capable of increasing discharges without raising the headwater level. Therefore, these are fine hydraulic structures for water control in reservoirs and irrigation systems. In addition, accurate C_d predictions prevent

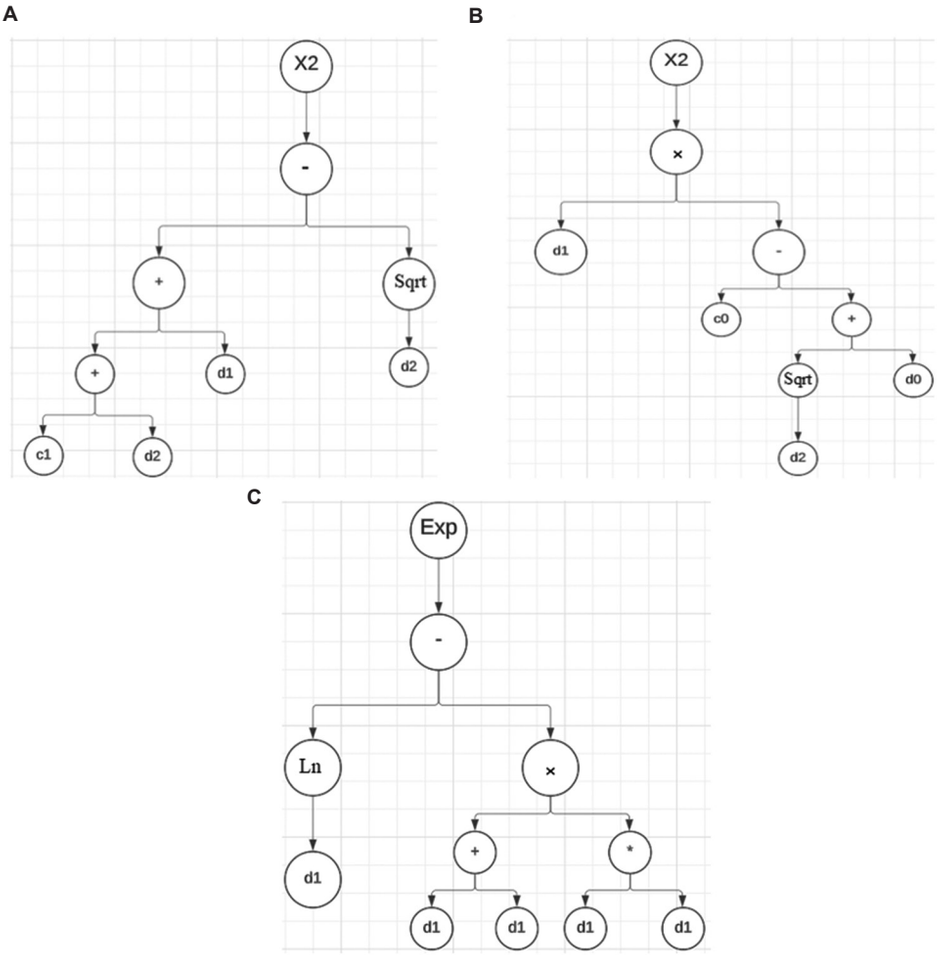

Figure 3. Developed gene expression programming output. (A) Sub-expression tree 1. (B) Sub-expression tree 2. (C) Sub-expression tree 3.

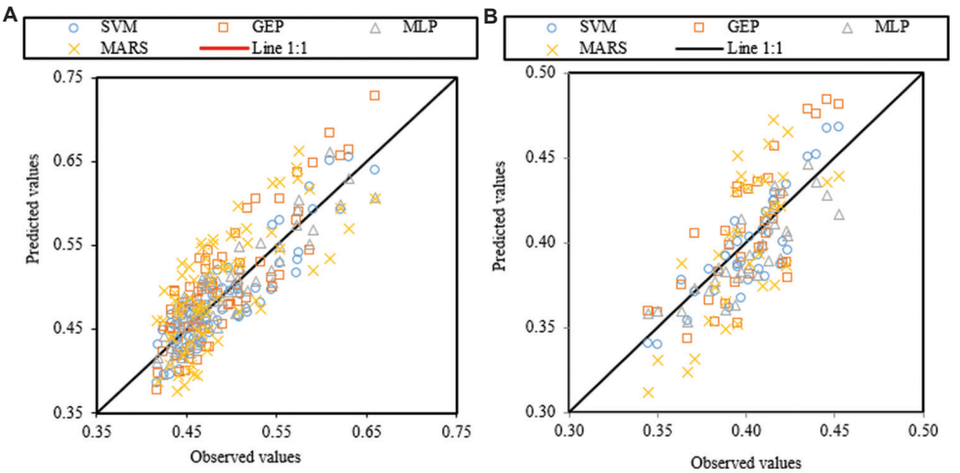

Figure 4. Scatter plots of the observed and predicted values of the C_d across the four models. (A) Training phase. (B) Testing phase.

Abbreviations: GEP: Gene expression programming; MARS: Multivariate adaptive regression splines; MLP: Multilayer perception; SVM: Support vector machine.

Table 7. Residual analysis of the machine learning models' outputs

Model	Training phase				Testing phase			
	Maximum	Minimum	Mean	Sum	Maximum	Minimum	Mean	Sum
SVM	0.0549	−0.041	0.006	0.454	0.0327	−0.022	0.004	0.140
GEP	0.0485	−0.078	−0.012	−0.862	0.0440	−0.043	−0.004	−0.146
MLP	0.0393	−0.052	−0.002	−0.140	0.0235	−0.028	0.002	0.086
MARS	0.0743	−0.090	−0.013	−0.902	0.0431	−0.071	−0.005	−0.191

Abbreviations: GEP: Gene expression programming; MARS: Multivariate adaptive regression splines; MLP: Multilayer perceptron; SVM: Support vector machine.

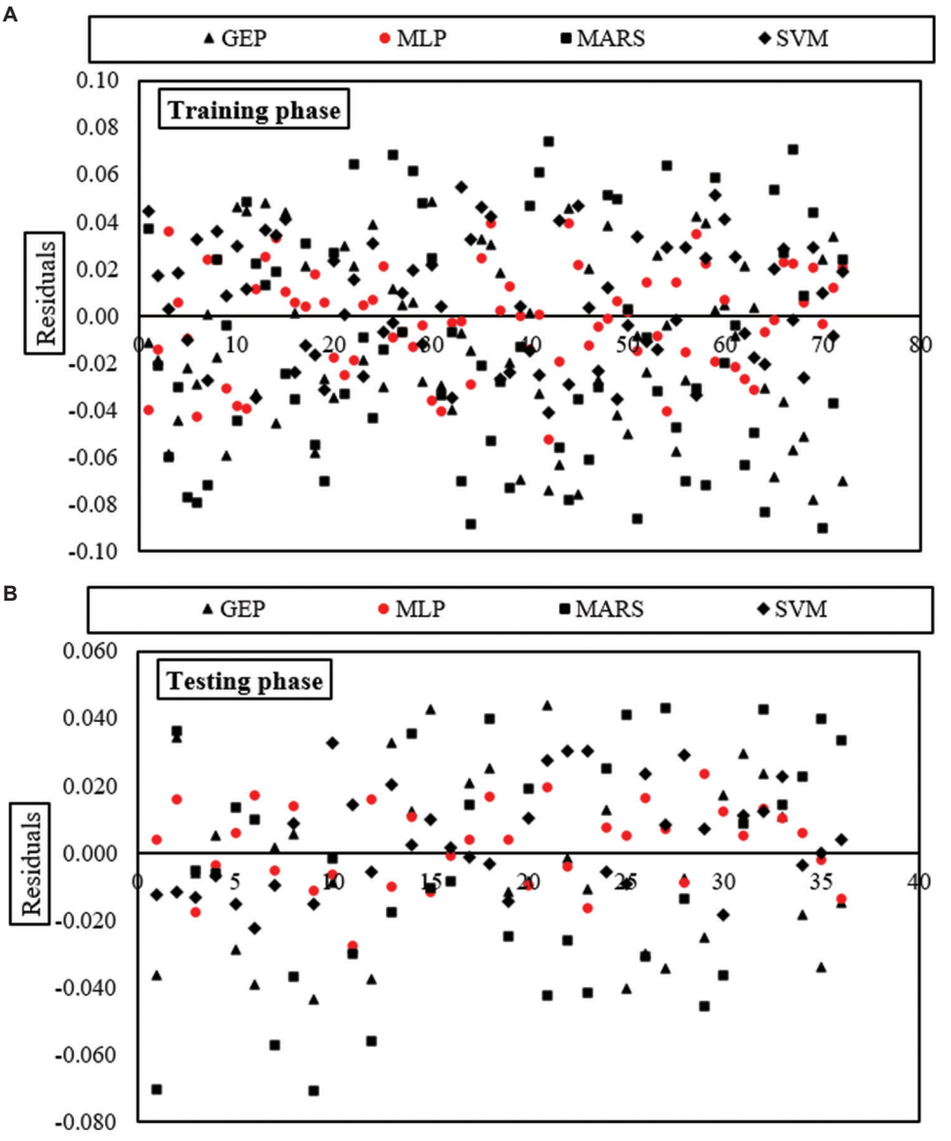

Figure 5. Residual error variation of the machine learning models' outcomes. (A) Training phase. (B) Testing phase.

Abbreviations: GEP: Gene expression programming; MARS: Multivariate adaptive regression splines; MLP: Multilayer perception; SVM: Support vector machine.

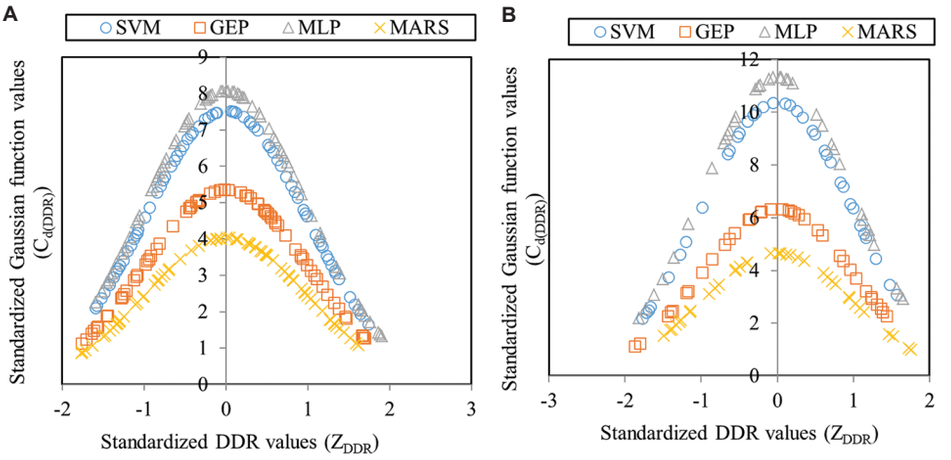

Figure 6. Performance assessment of the machine learning models' outcome using the DDR index. (A) Training phase. (B) Testing phase.

Abbreviations: GEP: Gene expression programming; MARS: Multivariate adaptive regression splines; MLP: Multilayer perception; SVM: Support vector machine.

overdesigns or underdesigns and save construction costs. They also allow proper overtopping from dams and prevent or mitigate dam failures in extreme weather conditions. Climate change has significantly enhanced the chances of extreme weather conditions; therefore, some of the hydraulic structures made for usual weather conditions might not withstand properly. Therefore, having an accurately predicted labyrinth weir in such conditions would be beneficial.

Ecosystem protection is another attribute of the properly designed labyrinth weir. Downstream soil erosion and excessive sediment transportation can be mitigated through the accurate prediction of C_d. These advantages are aligned with the Sustainable Development Goals (SDGs) – SDG6: clean water and sanitation, SDG9: industry, innovation, and infrastructure, SDG 11: sustainable cities and communities, SDG 13: climate action, and SDG 15: life on land. Therefore, the research presented here has a greater practical potential in achieving the SDGs. Furthermore, the impact on developing countries would be significant. Labyrinth weirs are more cost-effective compared to traditional spillways and offer greater benefits to rural communities facing water management challenges.

4. Conclusion

Given the pivotal significance of C_d in the operational efficacy of weirs, alongside the advancing application of data-driven models for predicting this coefficient, the avenue for forthcoming research in the domain of TALW is explored. The present research employed four distinct models – SVM, GEP, MLP, and MARS – to anticipate the C_d of TALW. The assessment of performance evaluation metrics, while affirming the capabilities of the quartet mentioned above, revealed the preeminence of the MLP model in contrast to its three counterparts. This ascendancy was consistently evident across both the training and testing phases. The outcomes underscored that the SVM, GEP, and MARS models secured successive positions as commendable simulators following the MLP model.

While this study provides robust MLMs for predicting C_d in TALW under controlled laboratory conditions, translating these findings to field applications faces inherent limitations. Laboratory models assume optimal structural integrity, whereas field structures are subjected to factors such as concrete erosion, joint displacement, and corrosion over time, which may alter their hydraulic performance. Furthermore, reservoir sedimentation and organic debris accumulation – both absent in lab settings – can reduce effective crest length and amplify local head losses, systematically biasing C_d. Field environments also introduce hydrologic uncertainties, such as stage measurement errors (e.g., gauge drift and thermal effects) and unsteady flow regimens not replicated in steady-state experiments. Critically, neglected maintenance (e.g., spillway cracking and gate misalignment) may induce unexpected flow behavior, as evidenced by real-world failures like the Oroville Dam incident in 2017,[52] where operational stresses exceeded design assumptions. These real-world complexities necessitate field validation of the models and the integration of probabilistic safety margins in

design protocols to account for infrastructure aging and measurement uncertainties.

Acknowledgments

None.

Funding

None.

Conflict of interest

Upaka Rathnayake is an Editorial Board Member of this journal but was not in any way involved in the editorial and peer-review process conducted for this paper, directly or indirectly. Separately, other authors declared that they have no known competing financial interests or personal relationships that could have influenced the work reported in this paper.

Author contributions

Conceptualization: Mohammad Heidarnejad, Jamal Feili
Formal analysis: Mehdi Fuladipanah
Methodology: Upaka Rathnayake, Mohammad Heidarnejad
Writing–original draft: Mehdi Fuladipanah
Writing–review & editing: Upaka Rathnayake, Mohammad Heidarnejad

Availability of data

The data that support the findings of this study are available on request from the corresponding author. The data are not publicly available due to privacy or ethical restrictions.

References

1. Afaridegan E, Amanian N, Parsaie A, Gharehbaghi A. Hydraulic investigation of modified semi-cylindrical weirs. *Flow Meas Instrum.* 2023;93:102405. doi: 10.1016/j.flowmeasinst.2023.102405
2. Bekheet AA, AboulAtta NM, Saad NY, El-Molla DA. Effect of the shape and type of piano key weirs on the flow efficiency. *Ain Shams Eng J.* 2022;13(3):101620. doi: 10.1016/j.asej.2021.10.015
3. Nourani B, Arvanaghi H, Pourhosseini FA, Javidnia M, Abraham J. Enhanced support vector machine with particle swarm optimization and genetic algorithm for estimating discharge coefficients of circular-crested oblique weirs. *Iran J Sci Technol Trans Civil Eng.* 2023;47(5):3185-3198. doi: 10.1007/s40996-023-01110-0
4. Roushangar K, Alami MT, Shiri J, Asl MM. Determining discharge coefficient of labyrinth and arced labyrinth weirs using support vector machine. *Hydrol Res*. 2018;49(3):924-938. doi: 10.2166/nh.2017.214
5. Taylor G. *The Performance of Labyrinth Weirs*. PhD Thesis. Nottingham, UK: University of Nottingham; 1968.
6. Hay N, Taylor G. Performance and design of labyrinth weirs. *J Hydraul Div.* 1970;96(11):2337-2357. doi: 10.1061/JYCEAJ.0002766
7. Lux F. Design and construction of labyrinth spillways. In: *15th Commission Internationale des Grands Barrages*. Ontario: Canadian Dam Association; 1985. p. 249-274.
8. Kocahan H, Taylor G. Rehabilitation of Black Rock Dam (Seepage & Inadequate Spillway). In: *Association of State Dam Safety Officials Conference*. Arlington, VA, USA; 2002.
9. Crookston BM, Tullis B. *Labyrinth Weirs*. *Hydraulic Structures*. Vol. 59. United States: Utah States University; 2010.
10. Christensen NA, Tullis BP. *Arced Labyrinth Weir Flow Characteristics*. United States: Utah States University; 2012.
11. Seamons TR. *Labyrinth Weirs: A Look into Geometric Variation and its Effect on Efficiency and Design Method Predictions*. United States: Utah State University; 2014.
12. Bijankhan M, Kouchakzadeh S. Unified discharge coefficient formula for free and submerged triangular labyrinth weirs. *Flow Meas Instrum.* 2017;57:46-56. doi: 10.1016/j.flowmeasinst.2017.08.007
13. Monjezi R, Heidarnejad M, Masjedi A, Purmohammadi MH, Kamanbedast A. Laboratory investigation of the discharge coefficient of flow in arced labyrinth weirs with triangular plans. *Flow Meas Instrum.* 2018;64:64-70. doi: 10.1016/j.flowmeasinst.2018.10.011
14. Seyedian SM, Haghiabi A, Parsaie A. Reliable prediction of the discharge coefficient of triangular labyrinth weir based on soft computing techniques. *Flow Meas Instrum.* 2023;92:102403. doi: 10.1016/j.flowmeasinst.2023.102403
15. Zare H, Vaghefi M, Mahmoudi A, Behroozi AM. Experimental exploration of flow hydraulics and discharge coefficient for an inclined circular labyrinth weir. *Water Resour Manag.* 2023;37(11):4521-4536. doi: 10.1007/s11269-023-03577-y
16. Nematollahi S, Izadinia E, Khoshfetrat A. Investigation of discharge coefficient and flow energy loss in sinusoidal-labyrinth weirs. *Iran J Sci Technol Trans Civil Eng.* 2025:1-10.

doi: 10.1007/s40996-025-01820-7
17. Ahmed AM, Altalib AN. Determination of discharge coefficient of arced labyrinth weir with semicircular openings. *Iran J Sci Technol Trans Civil Eng.* 2025:1-12. doi: 10.1007/s40996-025-01747-z
18. Masoudi MH, Yari A, Sadeghian J, Norouzi H. Experimental investigation of the discharge coefficient of the rectangular and trapezoidal labyrinth weirs considering variable congress lengths. *Model Earth Syst Environ.* 2024;10(2):2819-2832. doi: 10.1007/s40808-023-01925-w
19. Hadi ZM, Majeed HQ. Experimental and Numerical Study of the Discharge Capacity of a Labyrinth Side Weir in a Straight Channel. *In: AIP Conference Proceedings*. Vol. 3091. Melville, NY: AIP Publishing; 2024.
20. Darvas LA. Discussion of performance and design of labyrinth weirs, by Hay and Taylor. *J Hydraul Eng.* 1971;97:1246-51.
21. Lux F, Hinchliff D. Design and Construction of Labyrinth Spillways. *In: 15th Congress International Commission on Large Dams ICOLD*. Vol. 4. Lausanne, Switzerland: 1985. p. 249-274.
22. Melo JF, Ramos CM, Magalhães AP. Descarregadores Com Soleira em Labirinto de um Ciclo em Canais Convergentes. In: *Determinação da Capacidade de Vazão Proceedings 6th Congresso da Água*. 2002.
23. Crookston BM. *Labyrinth Weirs*. Doctor of Philosophy, Utah State University [PhD Dissertation]; 2010.
24. Emiroglu ME, Kaya N, Agaccioglu H. Discharge capacity of labyrinth side weir located on a straight channel. *J Irrig Drain Eng.* 2009;136(1):37-46. doi: 10.1061/(ASCE)IR.1943-4774.0000112
25. Karami H, Karimi S, Bonakdari H, Shamshirband S. Predicting discharge coefficient of triangular labyrinth weir using extreme learning machine, artificial neural network and genetic programming. *Neural Comput Appl.* 2018;29(11):983-989. doi: 10.1007/s00521-016-2588-x
26. Bonakdari H, Ebtehaj I, Gharabaghi B, Sharifi A, Mosavi A. Prediction of discharge capacity of labyrinth weir with gene expression programming. *In: Proceedings of SAI Intelligent Systems Conference*. Cham: Springer International Publishing; 2020. p. 202-217. doi: 10.1007/978-3-030-55180-3_17
27. Khani M, Shabanlou S. Assessment of discharge coefficient in trapezoidal and rectangular canals through regularized extreme learning machine. *Measurement*. 2021;180:109493. doi: 10.1016/j.measurement.2021.109493
28. Mahmoud A, Hu T, Zeng X, Jing P, Li X, Ribeiro EDC. Hydraulic informed multi-layer perceptron for estimating discharge coefficient of labyrinth weir. *Eng Appl Artif Intell.* 2023;123:106435. doi: 10.1016/j.engappai.2023.106435
29. Emami H, Emami S, Parsa J. A walnut optimization algorithm applied to discharge coefficient prediction on labyrinth weirs. *Soft Comput.* 2022;26:12197-12215. doi: 10.1007/s00500-022-07041-8
30. Majedi-Asl M, Fuladipanah M, Arun V, Tripathi RP. Using data mining methods to improve discharge coefficient prediction in piano key and labyrinth weirs. *Water Supply.* 2022;22(2):1964-1982. doi: 10.2166/ws.2021.304
31. Mustafa M, Mansoor T, Muzzammil M. Support vector machine (SVM) approach to develop the discharge prediction model for triangular labyrinth weir. *Water Supply.* 2022;22:8942-8956. doi: 10.2166/ws.2022.393
32. Wang F, Zheng S, Ren Y, Liu W, Wu C. Application of hybrid neural network in discharge coefficient prediction of triangular labyrinth weir. *Flow Measure Instrument.* 2022;83:102108. doi: 10.1016/j.flowmeasinst.2021.102108
33. Hu Z, Karami H, Rezaei A, *et al*. Using soft computing and machine learning algorithms to predict the discharge coefficient of curved labyrinth overflows. *Eng Appl Comput Fluid Mech.* 2021;15(1):1002-1015. doi: 10.1080/19942060.2021.1934546
34. Mahmoud A, Yuan X, Hajilounezhad T, Yuan Y. Investigation on labyrinth spillway multi-objective optimization with an emphasis on predicting discharge coefficient through different artificial neural networks. *Measurement*. 2021;174:109036. doi: 10.1016/j.measurement.2021.109036
35. Shafiei S, Najarchi M, Shabanlou SA. Novel approach using CFD and neuro-fuzzy-firefly algorithm in predicting labyrinth weir discharge coefficient. *J Braz Soc Mech Sci Eng.* 2020;42:44. doi: 10.1007/s40430-019-2109-9
36. Norouzi P, Rajabi A, Izadbakhsh MA, Shabanlou S, Yosefvand F, Yaghoubi B. A new non-tuned self-adaptive machine-learning approach for simulating the discharge coefficient of labyrinth weirs. *Irrig Drainag.* 2020;69(3):398-416. doi: 10.1002/ird.2423
37. Olyaie E, Banejad H, Heydari M. Estimating discharge coefficient of PK-weir under subcritical conditions based on high-accuracy machine learning approaches. *Iran J Sci Technol Trans Civil Eng.* 2019;43:89-101. doi: 10.1007/s40996-018-0150-z
38. Roushangar K, Alami MT, Shiri J, Asl MM. Determining discharge coefficient of labyrinth and arced labyrinth weirs using support vector machine. *Hydrol Res.* 2018;49(3):924-938. doi: 10.2166/nh.2017.214
39. Uyumaz A, Danandeh Mehr A, Kahya E, Erdem H. Rectangular side weirs discharge coefficient estimation in circular channels using linear genetic programming approach. *J Hydroinform.* 2014;16(6):1318-1330. doi: 10.2166/hydro.2014.112

40. Emiroglu ME, Kisi O. Prediction of discharge coefficient for trapezoidal labyrinth side weir using a neuro-fuzzy approach. *Water Resour Manag.* 2013;27:1473-1488. doi: 10.1007/s11269-012-0249-0
41. Cortes C, Vapnik V. Support-vector networks. *Mach Learn.* 1995;20:273-297. doi: 10.1007/BF00994018
42. Sandamal K, Shashiprabha S, Muttil N, Rathnayake U. Pavement roughness prediction using explainable and supervised machine learning technique for long-term performance. *Sustainability*. 2023;15(12):9617. doi: 10.3390/su15129617
43. Ferreira C. Gene expression programming: A new adaptive algorithm for solving problems. *Complex Syst*. 2001;13:87-129. doi: 10.48550/arXiv.cs/0102027
44. Fuladipanah M, Shahhosseini A, Rathnayake N, *et al*. In-depth simulation of rainfall-runoff relationships using machine learning methods. *Water Pract Technol.* 2024;19(6):2442-2459. doi: 10.2166/wpt.2024.147
45. Perera A, Hazi MD, Upaka R. Comparison of different artificial neural network (ANN) training algorithms to predict the atmospheric temperature in Tabuk, Saudi Arabia. *MAUSAM*. 2021;71(2):233-244. doi: 10.54302/mausam.v71i2.22
46. Agbasi JC, Egbueri JC. Prediction of potentially toxic elements in water resources using MLP-NN, RBF-NN, and ANFIS: A comprehensive review. *Environ Sci Pollut Res Int*. 2024;31:30370-30398. doi: 10.1007/s11356-024-33350-6
47. Lukas P, Melesse AM, Kenea TT. Predicting reservoir sedimentation using multilayer perceptron - artificial neural network model with measured and forecasted hydrometeorological data in gibe-III reservoir, omo-gibe river basin, Ethiopia. *J Environ Manag.* 2024;359:121018. doi: 10.1016/j.jenvman.2024.121018
48. Friedman JH. Multivariate adaptive regression splines. *Ann Statis.* 1991;19:1-67. doi: 10.1214/aos/1176347963
49. Garai S, Paul RK, Yeasin M, Paul AK. CEEMDAN-based hybrid machine learning models for time series forecasting using MARS algorithm and PSO-optimization. *Neural Process Lett.* 2024;56(2):92. doi: 10.1007/s11063-024-11552-w
50. Fuladipanah M, Azamathulla HM, Kisi O, Kouhdaragh M, Mandala V. Quantitative forecasting of bed sediment load in river engineering: An investigation into machine learning methodologies for complex phenomena. *Water Supply*. 2024;24(2):585-600. doi: 10.2166/ws.2024.017
51. Noori R, Khakpour A, Omidvar B, Farokhnia A. Comparison of ANN and principal component analysis-multivariate linear regression models for predicting the river flow based on developed discrepancy ratio statistic. *Expert Syst Appl.* 2010;37(8):5856-5862. doi: 10.1016/j.eswa.2010.02.020
52. Koskinas A, Tegos A, Tsira P, *et al*. Insights into the Oroville dam 2017 spillway incident. *Geosciences*. 2019;9(1):37. doi: 10.3390/geosciences9010037